

## Low dimensionality of the surface conductivity of diamond

Moritz V. Hauf, Patrick Simon, Max Seifert, Alexander W. Holleitner, Martin Stutzmann, and Jose A. Garrido\*  
*Walter Schottky Institute, Physik-Department, Technische Universität München, Am Coulombwall 4, 85748 Garching, Germany*  
 (Received 1 November 2013; published 19 March 2014)

Undoped diamond, a remarkable bulk electrical insulator, exhibits a high surface conductivity in air when the surface is hydrogen terminated. Although theoretical models have claimed that a two-dimensional hole gas is established as a result of surface energy-band bending, no definitive experimental demonstration has been reported so far. Here, we prove the two-dimensional character of the surface conductivity by low-temperature characterization of diamond in-plane gated field-effect transistors that enable the lateral confinement of the transistor's drain-source channel to nanometer dimensions. In these devices, we observe Coulomb blockade effects of multiple quantum islands varying in size with the gate voltage. The charging energy and thus the size of these zero-dimensional islands exhibit a gate-voltage dependence which is the direct result of the two-dimensional character of the conductive channel formed at hydrogen-terminated diamond surfaces.

DOI: [10.1103/PhysRevB.89.115426](https://doi.org/10.1103/PhysRevB.89.115426)

PACS number(s): 73.23.Hk, 73.25.+i, 73.63.Kv, 81.05.ug

### I. INTRODUCTION

Bulk diamond, with a band gap of  $E_{\text{gap}} = 5.45$  eV, is considered an insulator or wide band gap semiconductor. It therefore came as a big surprise when Landstrass and Ravi discovered high conductivity in undoped, chemical-vapor-deposited diamond films [1]. It took years until Maier *et al.* came up with an explanation, the so-called transfer-doping model [2], which is now widely accepted. It ascribes the diamond surface conductivity to the presence of a two-dimensional hole gas (2DHG) at a hydrogen-terminated diamond surface. The 2DHG is established as a result of two necessary conditions: first, a hydrogen termination of the diamond surface and, second, the presence of atmospheric adsorbates. The C-H dipoles of the H-terminated surface induce a negative electron affinity that effectively shifts the valence-band maximum closer to the vacuum level. The atmospheric adsorbates at the diamond surface provide acceptor states with energies  $\mu_{ec}$  that are low enough such that electrons can be extracted from the valence band. Thermal equilibrium yields a band bending at the diamond surface with an electrostatic potential well filled by free holes [Fig. 1(a)]. In contrast to the H-terminated diamond surface, the energy bands of an O-terminated surface lie around 2.7 eV lower, such that no 2DHG can be established and the surface remains insulating [3,4]. Based on this phenomenon, electronic devices such as diamond solution-gated field-effect transistors (SGFETs) have been developed [5,6], where an electrolyte serves as a top gate to modulate the surface conductivity. They have proven to be excellent candidates for the fabrication of biosensors, showing pH [7] and ion sensitivity [8], as well as being capable of detecting action potentials from cells [9] or neurotransmitters [10]. In addition, in-plane gated field-effect transistors (IPGFETs) have been demonstrated [11]. In these devices charge carriers are laterally depleted from a nanometer-sized H-terminated channel [12,13]. In the design of diamond-based IPGFETs, thin O-terminated potential barriers separate one or two side gate regions from a conductive H-terminated drain-source channel, as depicted in Fig. 1(b). The devices are

designed such that a drain-source current through the channel has to pass through a nanometer-sized constriction [Figs. 1(d) and 1(e)]. The electric field across the O-terminated potential barriers creates a depletion region which reduces the effective width  $w_{\text{eff}}$  of the drain-source channel [Fig. 1(b)].

In this paper, we employ in-plane gates to laterally reduce the dimensionality of the 2DHG at the H-terminated diamond surface. We directly prove the two-dimensional nature of the diamond surface conductivity by the observation of a 2D characteristic gate dependence of the Coulomb blockade effect in the drain-source channel conductance at liquid-helium temperature. These effects are the result of zero-dimensional quantum islands, electrostatically generated by the lateral gates in the narrow constriction of the channel.

### II. EXPERIMENTAL DETAILS

We used single-crystalline, electronic-grade diamond substrates (Element Six Ltd.) with an rms surface roughness below 1 nm. Hydrogen termination was achieved in a microwave reactor at 750 W, 700°C, and 100 SCCM (SCCM denotes cubic centimeter per minute at standard pressure) for 15 min, followed by a controlled cooldown at 230 W for 30 min. Bond pads are formed by evaporation of a 10 nm/100 nm Ti/Au metal layer on oxygen-terminated areas. The hydrogen-terminated conductive areas of the IPGFET are defined by selectively oxidizing the surrounding areas using an oxygen microwave reactor. Ohmic gold contacts were fabricated by a 100-nm Au layer, overlapping into the hydrogen-terminated conductive channel and defined by selective KI/I<sub>2</sub> etching. Conventional photolithography and electron-beam lithography were used to realize O-terminated lines with a minimum width of 100 nm and devices with a minimum channel width of around 50 nm. The scanning electron microscope (SEM) images in Figs. 1(d) and 1(e) depict two different surface termination patterns in the central region of a device. Two curved side gates [Fig. 1(e)] confine the channel from two sides, or only one side gate is used in a T-shaped design [Fig. 1(d)]. The latter provides a minimum channel length which is similar to the width of the O-terminated line. The low-temperature characterization was performed either in a liquid-helium bath or in vacuum in a closed-cycle

\*joseantonio.garrido@wsi.tum.de

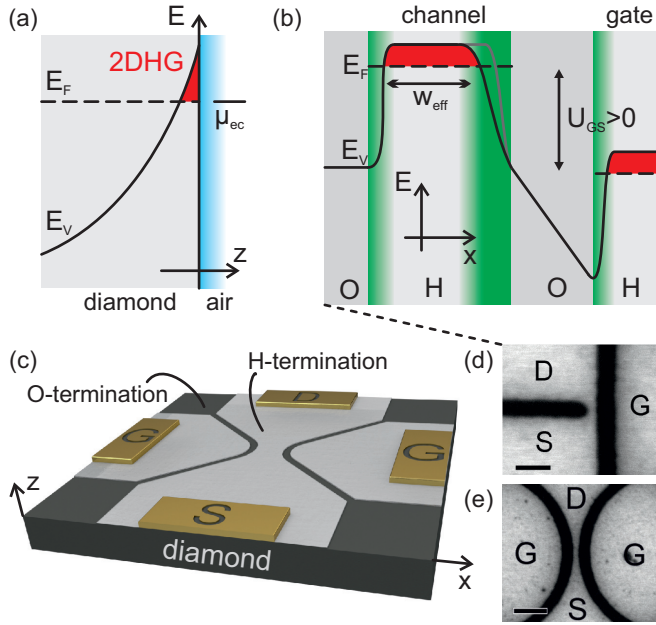


FIG. 1. (Color) Basic principles of a diamond in-plane gated field-effect transistor. (a) Energy-band schematic of a H-terminated diamond surface. Equilibration of  $E_F$  with  $\mu_{EC}$  leads to a bending of the valence-band edge and the creation of a 2DHG at the surface. (b) Energy-band schematic across the central region of the IPGFET. A positive  $U_{GS}$  increases the depletion region (green), reducing the effective width  $w_{\text{eff}}$  of the conductive channel. (c) Schematic of a diamond IPGFET with two curved side gates. SEM images of diamond IPGFET structures with (d) T-shaped single side gate and (e) two curved side gates. Scale bars are 200 nm.

cryostat at  $T \approx 8$  K. Lock-in techniques were used for the characterization of the devices.

### III. RESULTS

#### A. Room-temperature operation

We first investigated the diamond in-plane gated field-effect transistors at room temperature in air. Figure 2(a) shows the current-voltage characteristics of a 50-nm-wide diamond IPGFET (curved side gates) for gate-source voltages  $U_{GS}$  between  $-1.0$  and  $2.6$  V. As can be observed, the channel conductivity decreases with more positive gate voltages. Further, the transistor curves exhibit a linear dependence of the drain-source current  $I_{DS}$  on the drain-source voltage  $U_{DS}$  for low values of  $U_{DS}$  and saturation at higher values [Fig. 2(b)]. Figure 2(c) shows the gate-voltage dependence of the channel conductance  $G$ . The transistor is fully open when  $U_{GS} < 0$  V, showing a constant conductance. The channel starts to close linearly for more positive voltages until it is closed beyond the threshold voltage  $U_{th}$ , which is defined as the gate voltage where the extrapolation of the linear current regime equals zero. From the characterization of IPGFETs with channel widths of 50, 100, and 250 nm, we have confirmed a linear dependence of  $U_{th}$  on the lithographically designed channel width  $w_{\text{geo}}$ .

We can understand these results by using a basic description of the diamond in-plane gates following Refs. [11–13] and

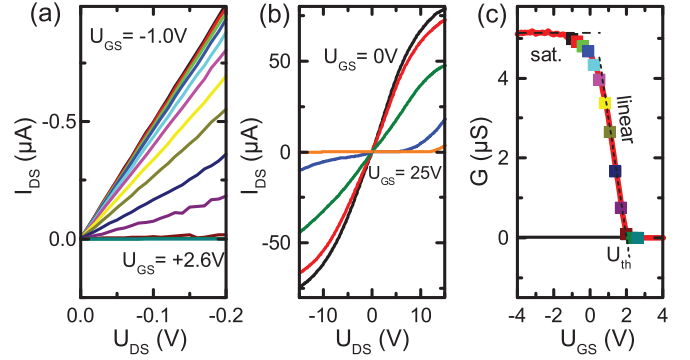


FIG. 2. (Color) Transistor characteristics of a diamond IPGFET at (a) small and (b) large values of  $U_{DS}$  for 50- and 250-nm channel widths, respectively. (c) Dependence of conductance  $G$  on the side gate voltage  $U_{GS}$  (50-nm channel width, curved side gates). Colored symbols correspond to the data in (a). The saturation region and linear region are indicated by dashed lines.

considering the energy-band schematic in Fig. 1(b). At the interface between the oxygen and hydrogen terminations, the energy bands are offset by a built-in potential  $eU_{bi}$ , which is governed by the different polarities of the surface dipoles in the absence of interfacial charge. Even at  $U_{GS} = 0$  V, the built-in voltage  $U_{bi}$  creates a small depletion region (green shaded areas) in the vicinity of the interface, similar to the case of a  $p$ - $n$  junction. The application of a gate voltage across the O-terminated potential barrier modifies the energy bands at the diamond surface, as shown in Fig. 1(b). Far away from any interface between the oxygen and hydrogen termination, the relative position of the valence-band edge  $E_{VBM}$  and the Fermi level  $E_F$  stays constant within the H-terminated regions. However, their absolute energy levels are offset by  $eU_{GS}$  when a gate voltage is applied across the O-terminated potential barrier. Close to the interface, the gate voltage modifies the energy-band bending. As a result, the extension of the depletion region  $w_{\text{dep}}^{2D}$  varies according to

$$w_{\text{dep}}^{2D} = \frac{\epsilon\epsilon_0}{en_h}(U_{bi} \pm U_{GS}), \quad (1)$$

as described by Petrosyan and Shik for a two-dimensional system [14]. Here,  $\epsilon$  and  $\epsilon_0$  are the dielectric constants of diamond and vacuum, respectively,  $e$  is the elementary charge, and  $n_h$  is the carrier concentration ( $\text{cm}^{-2}$ ) in the 2DHG. The voltage-governed increase of the depletion region [Eq. (1)] linearly reduces the effective channel width  $w_{\text{eff}} = w_{\text{geo}} - 2w_{\text{dep}}^{2D}$ . This is directly reflected in the linear decrease of the channel conductance with the gate voltage, as observed experimentally [Fig. 2(c)]. We can understand  $U_{th}$  as the voltage where  $w_{\text{eff}} = 0$ . In addition, the linearity of  $w_{\text{dep}}^{2D}$  is in good agreement with the observed linear dependence of  $U_{th}$  on  $w_{\text{geo}}$ . Saturation of the conductance is observed for negative  $U_{GS}$ , as the channel cannot be made wider than its lithographic width ( $w_{\text{eff}} = w_{\text{geo}}$ ).

Current saturation observed at large values of  $U_{DS}$ , as depicted in Fig. 2(c), can be attributed to charge-carrier velocity saturation, as the saturation effect is observed for both  $U_{DS}$  polarities. For a two-sided gate structure we can estimate the drift saturation velocity  $v_{d,\text{sat}}$  using the definition of the

effective channel width  $w_{\text{eff}}$  and Eq. (1):

$$\frac{\partial I_{DS,\text{sat}}}{\partial U_{GS}} = en_h v_{d,\text{sat}} \frac{\partial w_{\text{eff}}}{\partial U_{GS}} = 2\epsilon\epsilon_0 v_{d,\text{sat}}. \quad (2)$$

Determining  $\partial I_{DS,\text{sat}}/\partial U_{GS}$  from Fig. 2(c) gives a drift saturation velocity of  $5 \times 10^6 \text{ cm s}^{-1}$ , which compares well to previously reported values [12].

### B. Low-temperature operation

We further characterized the diamond IPGFETs at liquid-helium temperatures to allow quantum effects to become observable. Figure 3(a) shows the gate-voltage dependence of the drain-source current. As shown at room temperature, the channel closes for more positive  $U_{GS}$ . However, a variety of oscillatory peaks in  $I_{DS}$  are visible. For a detailed investigation we measure the differential conductance  $g = \partial I_{DS}/\partial U_{DS}$  for different combinations of  $U_{DS}$  and  $U_{GS}$  [Fig. 3(b)]. Unlike at room temperature,  $I_{DS}$  does not show an Ohmic behavior with

$U_{DS}$  [ $g(U_{DS}) = \text{const}$ ]. There exists a central, nonconductive region (purple) which increases in size when the channel closes, i.e., at more positive  $U_{GS}$ . On the large gate-voltage scale, the edge of the purple region does not appear smooth; instead, Coulomb diamonds appear, as will be discussed in the following. The green line ( $g \approx 0.8 \mu\text{S}$ ) parallel to the edge of purple region is a measurement artifact and will be ignored in the following discussion.

We attribute our observations to Coulomb blockade effects in the nanometer-sized central region of the diamond IPGFETs. Coulomb blockade is observed when a small conductive region is separated by tunneling barriers from the drain and source contact [15]. Due to the small size of the quantum island, it shows discrete charging energies with an energy level spacing of  $e^2C^{-1}$ , where  $C$  is the capacitance of the island. An electron can only tunnel from the source into the island if the island's energy level is aligned or below the electrochemical potential of the source contact. From the island, it can only tunnel out if the drain level is below the energy level of the Coulomb island. As a result, there exist situations where charge transport across the island is blocked (Coulomb blockade) [15]. Coulomb diamonds are the graphical 2D representation of these regions when plotting the differential conductance  $g$  versus  $U_{DS}$  and  $U_{GS}$ .

In order to develop a better understanding and to support our claim, Fig. 3(c) shows the calculated charging energy inferred from the extension of the nonconductive region in Fig. 3(b). In the case of a 2D conductive layer, the capacitance  $C$  of a single Coulomb island with a circular disk shape is related to the island's radius  $r$  via  $C = 8\epsilon\epsilon_0 r$  [16]. A large charging energy of 49 meV is measured at around  $U_{GS} = 0 \text{ V}$ , which corresponds to an island radius of about 8 nm. The radius increases gradually as more negative voltages start to open the transistor channel until the tunneling barriers of the island vanish and the channel exhibits an Ohmic behavior at  $U_{GS} = -7 \text{ V}$ . Between  $-3.6$  and  $-0.4 \text{ V}$  a linear dependence of  $r$  on  $U_{GS}$  is observed. Since the radius is coupled to the quantum island charging energy  $e^2C^{-1}$  via the capacitance,  $C \propto r$ , an inverse proportionality of the charging energy on  $U_{GS}$  can be observed in the same region. Such a gate-voltage dependence of the charging energy and the radius is characteristic of a 2D conductive channel, as explained below. Let's start by assuming that the island's radius depends directly on the size of the depletion region via  $r = r_{\text{max}} - w_{\text{dep}}^{\text{2D}}$ . Here,  $r_{\text{max}}$  is some maximum value for the radius of the island. In a first approximation, the radius is assumed to decrease by the same amount that the depletion region increases in size. Based on this assumption and using Eq. (1), we can now estimate the carrier concentration from the slope of a linear fit of  $r$  in the region between  $-3.6$  and  $-0.4 \text{ V}$ , which results in a value around  $n_h \approx 4 \times 10^{12} \text{ cm}^{-2}$ . For an independent confirmation of this value, we have performed transport measurements using Hall bar structures on comparable diamond substrates and with the same fabrication technology as described above. In these experiments, a carrier concentration of  $n_h = 9 \times 10^{12} \text{ cm}^{-2}$  could be determined, which compares well to the value inferred from the gate-voltage dependence of the Coulomb island radius.

Figure 4(a) corresponds to a zoom of Fig. 3(b), revealing in more detail the presence of overlapping Coulomb diamonds

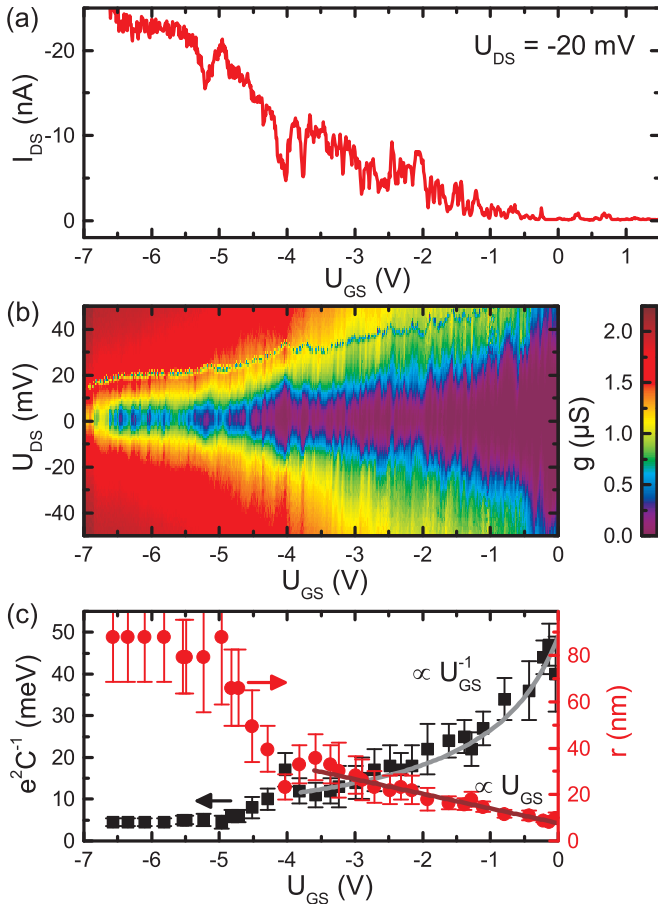


FIG. 3. (Color) Low-temperature characterization of a diamond IPGFET. (a) Gate-voltage dependence of the drain-source current  $I_{DS}$  at  $U_{DS} = -20 \text{ mV}$ . (b) Color map of the differential conductance  $g$  for different gate and drain-source voltages,  $U_{GS}$  and  $U_{DS}$  (two-sided curved gates, 50-nm width,  $T \approx 8 \text{ K}$ ). (c) Evaluation of the charging energy  $e^2C^{-1}$  of the Coulomb diamonds in (b). A gray line indicates a  $U_{GS}^{-1}$  proportionality. The radius  $r$  is calculated assuming a circular disk shape of the quantum dot. From the linear fit, indicated by a dark red line, the 2DHG carrier density can be calculated.

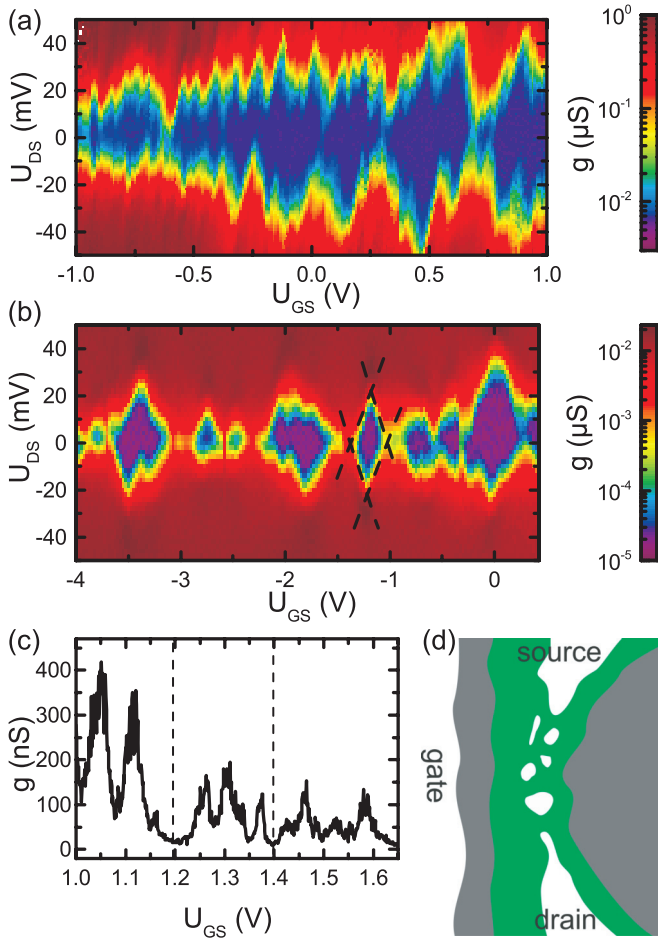


FIG. 4. (Color) Complex pattern of Coulomb diamonds resulting from coupled multiple quantum dots. (a) Coulomb diamonds in a two-sided curved gate structure. The sample is the same as in Fig. 3(b). (b) Coulomb diamonds in a T-shaped gate structure of 50-nm width at  $T = 6$  K. Dashed black lines are guides to the eye. (c) Coulomb blockade peaks in a similar device ( $U_{DS} = -10$  mV), revealing an arrangement of the peaks in three groups with three peaks each. (d) Schematic top view of the central channel region. The dark gray regions represent the O-terminated areas, whereas the green region sketches the extent of the depletion region. Several conductive islands (white regions) can be formed in the constriction between drain and source due to technology-related imperfections.

with a rather periodic gate dependence. Figure 4(b) shows a similar scan but for a T-shaped single side gate exhibiting a much shorter channel length. Here, individual Coulomb diamonds can be clearly identified, as well as overlapping diamonds. From the height of the individual Coulomb diamond at  $U_{GS} = -1.2$  V a capacitance of  $C = 7.3$  aF and a radius of  $r = 18$  nm can be derived. The different slopes of the Coulomb diamond edges indicate an asymmetry of the tunneling barriers between the quantum island and the drain and source contacts [17]. Figure 4(c) shows a high-resolution scan of  $g$  at  $U_{DS} = -10$  mV for a different sample but with the same channel geometry. No regular spacing of Coulomb peaks is observed, as would be expected for a single quantum dot [16,18]. However, the amplitude and spacing of the peaks suggests three groups with three peaks each. We tentatively attribute this observation

to the multidot splitting which Waugh *et al.* have observed for three electrically coupled quantum dots in series [19]. Figure 4(c) attempts to sketch a more realistic picture of a diamond in-plane gated (T-shaped) structure close to the threshold voltage. Between the depletion zone (green) from the built-in voltage and the depletion zone created by the gate, several conductive islands are localized in the center of the in-plane gate FET structure. The existence of multiple islands of varying shapes and sizes can be understood considering the following aspects. First, the lithographically designed O-terminated regions of the diamond surface (dark gray regions) show a less than perfect shape due to irregular broadening of the electron beam resist during O-plasma exposure. Second, the surface might have an imperfect hydrogen termination, creating an inhomogeneous potential landscape. Increasing the size of the depletion region via the applied  $U_{GS}$  will isolate Coulomb islands step by step from the drain or source regions, while continuously changing the dimension of the island. As a result, not only the electrochemical potentials of the individual islands but also the interlevel spacing of their charging energies are changed. In addition, the size and height of the tunneling barriers between the islands are influenced and therefore the interisland capacitances. Very similar effects have been observed in graphene nanoribbons [20,21]. An irregular arrangement of quantum dots which are interconnected in series and in parallel will yield a complex pattern of Coulomb diamonds [20]. This can explain the oscillatory edge of the nonconductive region in Fig. 3(b) that results from an overlap of Coulomb diamonds with varying sizes and shapes. Here, the long drain-source channel between the curved side gates allows several conductive islands to form. In this situation, our system starts to appear like a granular electronic system [22]. However, in our system the number of islands depends strongly on the gate voltage. At high negative  $U_{GS}$  the channel has opened so much that just one single conductive island remains. This island seems to keep a constant size, as revealed by the constant charging energy observed for large negative voltages in Fig. 3(c). In this situation,  $U_{GS}$  mostly tunes the electrochemical potential of the dot, leading to the rather periodic Coulomb diamond spacing observed between  $U_{GS} = -5.8$  and  $-6.8$  V. In comparison, the T-shaped single gate structures used to record Fig. 4(b) provide a much shorter channel length. Here, a lower number of conductive islands can be created, which results in more distinct Coulomb blockade effects from only a few islands [19,20].

#### IV. CONCLUSION

In conclusion, we have fabricated in-plane gated FETs on H-terminated diamond with nanometer-sized channel dimensions. Using the lateral control provided by the in-plane gates, it is possible to reduce the effective channel width until a Coulomb island with dimensions down to 10 nm is formed, revealing Coulomb blockade effects at low temperature. We could confirm that the electrostatic control of the island dimensions via the gate voltage shows a dependence characteristic of a 2D carrier density, confirming the two-dimensionality of the diamond's surface conductive channel observed in hydrogenated diamond.

## ACKNOWLEDGMENTS

The authors acknowledge the support of Markus Stallhofer and the financial support of the Graduate School for Complex

Interfaces (CompInt), TUM.solar in the frame of the Bavarian Collaborative Research Project “Solar Technologies go Hybrid” (SolTec), the Nanosystems Initiative Munich (NIM), and the DFG (Diamant Forschergruppe, 1492).

- 
- [1] M. I. Landstrass and K. V. Ravi, *Appl. Phys. Lett.* **55**, 1391 (1989).
- [2] F. Maier, M. Riedel, B. Mantel, J. Ristein, and L. Ley, *Phys. Rev. Lett.* **85**, 3472 (2000).
- [3] F. Maier, J. Ristein, and L. Ley, *Phys. Rev. B* **64**, 165411 (2001).
- [4] J. A. Garrido, A. Härtl, M. Dankerl, A. Reitingger, M. Eickhoff, A. Helwig, G. Müller, and M. Stutzmann, *J. Am. Chem. Soc.* **130**, 4177 (2008).
- [5] H. Kwarada, Y. Araki, T. Sakai, T. Ogawa, and H. Umezawa, *Phys. Status Solidi A* **185**, 79 (2001).
- [6] M. Dankerl, A. Lippert, S. Birner, E. U. Stützel, M. Stutzmann, and J. A. Garrido, *Phys. Rev. Lett.* **106**, 196103 (2011).
- [7] J. A. Garrido, A. Härtl, S. Kuch, M. Stutzmann, O. A. Williams, and R. Jackmann, *Appl. Phys. Lett.* **86**, 073504 (2005).
- [8] A. Härtl, J. A. Garrido, S. Nowy, R. Zimmermann, C. Werner, D. Horinek, R. Netz, and M. Stutzmann, *J. Am. Chem. Soc.* **129**, 1287 (2007).
- [9] M. Dankerl, S. Eick, B. Hofmann, M. Hauf, S. Ingebrandt, A. Offenhäusser, M. Stutzmann, and J. A. Garrido, *Adv. Funct. Mater.* **19**, 2915 (2009).
- [10] A. Härtl, E. Schmich, J. A. Garrido, J. Hernando, S. C. Catharino, S. Walter, P. Feulner, A. Kromka, D. Steinmüller, and M. Stutzmann, *Nat. Mater.* **3**, 736 (2004).
- [11] A. D. Wieck and K. Ploog, *Appl. Phys. Lett.* **56**, 928 (1990).
- [12] J. A. Garrido, C. E. Nebel, R. Todt, G. Rösel, M.-C. Amann, M. Stutzmann, E. Snidero, and P. Bergonzo, *Appl. Phys. Lett.* **82**, 988 (2003).
- [13] J. A. Garrido, C. E. Nebel, R. Todt, M.-C. Amann, O. A. Williams, R. Jackman, M. Nesládek, and M. Stutzmann, *Phys. Status Solidi A* **199**, 56 (2003).
- [14] S. Petrosyan and A. Y. Shik, *Sov. Phys. Semicond.* **23**, 696 (1989).
- [15] C. W. J. Beenakker and H. van Houten, *Solid State Phys.* **44**, 1 (1991).
- [16] A. Tilke, *Prog. Quantum Electron.* **25**, 97 (2001).
- [17] F. J. Kaiser, S. Kohler, P. Hänggi, M. Malecha, J. Ebbecke, A. Wixforth, H. W. Schumacher, B. Kästner, D. Reuter, and A. D. Wieck, *J. Phys.: Condens. Matter* **20**, 374108 (2008).
- [18] M. A. Kastner, *Rev. Mod. Phys.* **64**, 849 (1992).
- [19] F. R. Waugh, M. J. Berry, D. J. Mar, R. M. Westervelt, K. L. Campman, and A. C. Gossard, *Phys. Rev. Lett.* **75**, 705 (1995).
- [20] P. Gallagher, K. Todd, and D. Goldhaber-Gordon, *Phys. Rev. B* **81**, 115409 (2010).
- [21] F. Sols, F. Guinea, and A. H. Castro Neto, *Phys. Rev. Lett.* **99**, 166803 (2007).
- [22] I. Beloborodov, A. Lopatin, V. Vinokur, and K. Efetov, *Rev. Mod. Phys.* **79**, 469 (2007).